Synergistic effect of hydration and carbonation of ladle furnace slag on cementitious substances

Yuanrong Yi (yyrhyw@163.com)
Xinjiang University

Wenqing Ma
Xinjiang University

Ainiwaer Sidike
Xinjiang University

Zhongle Ma
Xinjiang University

Minghang Fang
Xinjiang University

Yue Lin
Xinjiang University

Shuqi Bai
Xinjiang University

Yinguang Chen
Tongji University

Article

Keywords: Ladle furnace slag, hydration and carbonation, 29Si NMR, C-S-H gel

Posted Date: April 11th, 2022

DOI: https://doi.org/10.21203/rs.3.rs-1529959/v1

Abstract

Ladle furnace slag (LFS) can undergo hydration and carbonation reactions as cement. This article explores the effect of LFS hydration and carbonation reactions on cementitious substances at different temperatures or different particle sizes, as well as the microstructure and formation mechanism of the cementitious substances. The results show that C_2S and C_3S undergo hydration reaction to generate C-S-H gel in the early stages, which then undergoes decalcification and condensation to generate $CaCO_3$ and Ca-deficient C-S-H gel. The increase in temperature hinders the formation of $CaCO_3$ from Ca^{2+} and CO_3^{2-}, thus reducing the efficiency of hydration carbonation. The increase in particle size is not conducive to leaching of C_2S and C_3S to the surface of the reaction phase, which in turn reduces the degree of decalcification and polymerization of C-S-H gel in the carbonation phase. It were concluded that the best hydration and carbonation reactions of LFS were achieved at 20 °C and particle sizes < 38 μm.

Highlights

·The best hydration and carbonation reactions occurred at 20 °C and particle sizes < 38 μm.

·C_2S and C_3S eventually formed $CaCO_3$ and Ca-deficient C-S-H gel.

·Reducing temperature and particle size facilitates the formation of cementitious substances.

·Hydration reaction and carbonation reactions promote and influence each other.

Introduction

Ladle furnace slag (LFS) produced as a by-product of secondary refining processes in the iron and steel industry, is an alkaline solid waste with high calcium content1. The mineral phase components of LFS mainly contain calcium metasilicate ($CaSiO_3$, CS), dicalcium silicate (Ca_2SiO_4, C_2S), tricalcium silicate (Ca_3SiO_5, C_3S), and free calcium oxide (f-CaO)2. LFS exhibits poor stability and poor compactness due to the high content of f-CaO. In addition, it exerts a filler effect that can densify the cementitious substances, because its mineral phase composition is similar to that of Ordinary Portland cement (OPC), that is all oxides present in LFS are also present in OPC, and exhibits the advantages of high affinity to cement-based materials and high abundance3. LFS added to cement-based materials as a mineral additive can accelerate the hydration reaction and increase the formation of hydration products such as calcium silicate hydrate (C-S-H) gel4. As the most important hydration product of cement slurries, C-S-H gel is an important source of mechanical properties in cementitious materials and considerably influences the carbonation of LFS and the preparation of cement 5.

The calcium-based substances in LFS exhibit good carbonation performance with a theoretical carbonation efficiency of 30–60%6. The poor stability and poor compactness of LFS can be mitigated by absorbing CO_2 to produce stable calcium carbonate ($CaCO_3$). Xu7 used CO_2 to immobilize heavy metals

in LFS and enhance its strength. Monkman8 estabished that the extractable CaO content of carbonated LFS compared with uncarbonated LFS was reduced by about 95%, which resulted in greatly improved strength after being convered into mortar, Therefore, carbonation can not only effectively achieve CO_2 storage but also improve the compressive strength of the final product. In the early stage of carbonation, the cementitious substancess C_2S and C_3S present in LFS undergo hydration reactions to form C-S-H gel. When comparing the changes of C-S-H gel during natural carbonation or accelerated carbonation, Auroy9 concluded that $CaCO_3$ was more conducive to forming crystalline spherical aragonite with a relatively stable structure after accelerated carbonation. Therefore, hydration and carbonation influences the composition of the cement-based materials and should be thoroughly studied.

Huijgen10 analyzed the controlling factors that affect the carbonation reaction, including particle size, temperature, solid-liquid ratio, stirring speed, and aeration rate and demonstrated that temperature and particle size are the two most important factors. Ashraf11 compared the carbonation process of CS, C_2S, and C_3S at different temperatures, reporting that the reactivity of CS samples was lower than that of C_2S and C_3S samples. Previous studies12, 13 reported that reducing the average particle size of slag can shorten the leaching channels from the metal ion core to the inner surface, thus promoting the utilization of slag and interactions between the slag-water-gas system. Suh14 reported that heating anhydrous calcium silicate clinker to 200°C resulted in a gradual increase in the Q_1 (SiO_4 tetrahedra connected to a SiO_4 tetrahedra) and Q_2 (SiO_4 tetrahedra connected to two SiO_4 tetrahedra) peak intensities obtained by deconvolution of the recorded ^{29}Si solid-state nuclear magnetic resonance (NMR) spectrum. Suh's results show that the hydration reaction of anhydrous calcium silicate can be accelerated by increasing the reaction temperature within a certain range. The aforementioned studies have generally assessed the effects of the hydration and carbonation reactions on mineral phase composition in isolation. However, only a few reports combine both reactions to analyze the change mechanism of the cementitious substances in dependence of temperature and particle size.

In this study, changes in the hydration reaction of C_2S and C_3S and the carbonation reaction of C-S-H gel in LFS when applying different temperatures and particle sizes are explored using solid-state ^{29}Si NMR technology. The samples were characterized by scanning electron microscopy (SEM), thermogravimetry (TG) and differential thermogravimetry (DTG), X-ray diffraction (XRD), and Brunner-Emmet-Teller (BET) analysis of nitrogen adsorption-desorption isotherms. Peak Fit software was used to analyze the changes in the cementitious substances during the hydration and the carbonation stage and revealed the formation mechanism of their microstructure. With the present work we aimed at understanding the effect of different temperatures or particle sizes on cementitious substances subjected to the hydration and carbonation reaction, and providing certain theoretical guidance for the application of LFS and LFS-based cement materials.

Materials And Methods

Experimental materials

The LFS used in the experiments was taken from a steel plant in Xinjiang(China), with the chemical composition and material shown in Table 1 and Fig. 1, respectively. The following XRD analysis shows that the main mineral phase components of the LFS include CS, C_2S, C_3S, and $CaAl_2Si_2O_8$. The lump LFS material was pulverized using a jaw crusher (BB200, Retsch, Germany) and then ground with a vibrating disc grinder (RS200, Retsch, Germany). Varying particle sizes were obtained by passing the ground sample through 180 μm, 96 μm, 48 μm, and 38 μm pore size sieves prior to the experiments.

Table 1. Chemical composition (by % weight) of the original LFS

Component	CaO	Al_2O_3	SiO_2	MgO	F	TiO_2	Na_2O	Fe_2O_3	MnO	Others
Content	62.32	18.64	8.45	4.26	3.65	0.81	0.083	0.746	0.20	0.83

Experimental process

A three-phase reaction tank was employed to investigate the influence of particle size and temperature on the carbonation of LFS. A slurry of LFS of the respective particle size was prepared with a solid-liquid ratio of 1:5 and used in the experiment at a CO_2 ventilation rate of 500 mL/min under stirring at 700 rad/min. Hydration and carbonation reactions were considered to be complete when the mass remained constant. To determine the influence of particle size, slurries with LFS particles sizes of 96-180 μm, 48-96 μm, 38-48 μm, < 38 μm were used at a reaction temperature of 20 ℃. To analyze the influence of temperature, samples with a particle size smaller than 38 μm were reacted at 20 ℃, 40 ℃, 60 °C, and 80 °C. At the end of the experiment, the solids in the slurry were separated from the liquid and dried at 105 °C for 8 hours to obtain carbonation products for analysis.

Characterization methods

X-ray diffraction analysis was performed to identify carbonation products using an X-ray powder diffractometer (D8 Advance, Bruker, Germany). For all materials, two samples were analyzed under the following experimental conditions: Cu Kα radiation (λ=0.154 nm), scanning range of 10-70°, scanning rate of 2.0°/min. The mineral phase composition was determined via thermal stability analysis (TG-DTG) using a simultaneous thermogravimetric analyzer (STA 7300, Hitachi, Japan) with 10 mg of sample analyzed at a temperature range from ambient temperature to 900 °C at a heating rate of 10 °C/min in a single measurement because variations in outcome are expected to be small15. A scanning electron microscope (LEO 1430VP, Carl Zeiss, Germany) was used at an accelerating voltage of 15 kV to analyze the micro-morphology of samples, which were sprayed with gold before the test to stabilize the image. Analysis of the microstructure changes during C_2S and C_3S carbonation was carried out via ^{29}Si NMR analysis (600M spectrometer, Agilent, US), with a 4-mm ZrO2 rotor using a rotation speed of 8 kHz and TMS solution as 29Si chemical shift calibration reference.

Results And Discussion

XRD analysis of the hydration and carbonation reaction

Fig. 2 shows the XRD patterns of LFS samples (< 38 μm) hydrated and carbonated at different temperatures and of LFS samples of different particle sizes after reaction at 20 ℃. The results confirm that LFS is an alkaline solid waste material composed mainly of silicate minerals, such as CS, C_2S, and C_3S, with additional amounts of calcium hydroxide $Ca(OH)_2$ and anorthite ($CaAl_2Si_2O_8$). After the hydration and carbonation reaction processes, the diffraction peaks of the calcium silicate phases were decreased or even disappeared. Simultaneously, three diffraction peaks appeared at around 2θ = 28.5°, 31.2°, and 61.2°, which were assigned to C-S-H gel 16-19, indicating that the calcium silicate phases formed C-S-H gel during the hydration and carbonation reaction. As C_2S and C_3S are known to undergo hydration reactions20, C_2S and C_3S present on the surface of LFS particles can undergo hydration to form C-S-H gel in the early stage of the reaction. As the reaction progresses, the C-S-H gel releases Ca^{2+} to maintain the required alkaline environment21, resulting in decalcification of the C-S-H gel. CO_2 gas was continuously passed through the solution to generate H_2CO_3 of weak acidity, which is extremely unstable and rapidly ionize in solution to generate HCO_3^- and CO_3^{2-}. The free Ca^{2+} in the solution combines with CO_3^{2-} to form stable $CaCO_3$. C-S-H gel will eventually provide more Ca^{2+} than the present $Ca(OH)_2$ when cement paste is exposed to high concentrations of CO_{222}, Finally, Ca^{2+} in $CaCO_3$ mainly originates from the hydration product C-S-H gel, and since the presence of moisture is a necessary condition to initiate the carbonation reaction23, 24, hydration will occur before the carbonation reaction. The XRD spectra in Fig. 2 indicate the formation of large amounts of $CaCO_3$ in the reaction at different temperatures or different LFS particle sizes, indicating that the main product after carbonation was $CaCO_3$. As CS cannot undergo a hydration reaction11, 25, 26, the CS present on the surface of LFS particles does not form C-S-H gel in the early stage of the reaction, but instead directly combines with CO_3^{2-} in solution to form $CaCO_3$. In addition, the diffraction peaks for $CaAl_2Si_2O_8$) did not change significantly following the hydration and carbonation reaction, indicating that the anorthite structure was relatively stable and did not participate in the reaction process, which is consistent with the results observed by Ashraf27. With the increase in reaction temperature, the $CaCO_3$ diffraction peaks gradually decrease, which may be due to faster movement of CO_2 molecules and expansion of the volume, resulting in an increase in the distance between the molecules of CO_2 and H_2O, weakening the intermolecular forces and hindering the generation of CO_3^{2-}[28]. In addition, the increase in temperature also causes the solubility of CO_2 to gradually decrease29, which ultimately leads to a reduction in carbonation efficiency. With the decrease in particle size, the diffraction peaks of the calcium silicate phases and $Ca(OH)_2$ gradually decrease, which might be explained by the simultaneously increasing surface area enhancing the contact area between particles and the solution which is conducive for the rate of the occurring reactions. However, a considerable amount of calcium silicates and $Ca(OH)_2$ did not participate in the hydration and carbonation reaction at the largest particle size of LFS, resulting in an incomplete reaction.

TG-DTG analysis of the hydration and carbonation reaction

Table 2. Changes in mineral phase composition determined by TG and RIR at different hydration and carbonation reaction temperatures or particle sizes

Carbonation periods		Uncarbonated	20 °C	40 °C	60 °C	80 °C	96-180 μm	48-96 μm	38-48 μm	38 μm
TG(%)	$CaCO_3$	-	24.7	25.1	24.6	18.0	1.0	20.0	21.8	24.7
	Total	1.9	35.2	35.2	34.4	27.3	2.1	29.2	32.9	35.2
RIR(%)	$CaCO_3$	-	23.0	22.9	23.1	23.3	6.3	18.0	19.2	23.0
	C_2S, C_3S	-	26.0	32.5	34.8	52.6	64.4	32.4	26.0	26.0

Fig. 3 shows the TG-DTG diagram of LFS after hydration and carbonation under different reaction temperatures or when different particle sizes were used. The mass losses are divided into three temperature ranges of 100-300 °C, 300-500 °C, and 500-850 °C, which are attributed to the dehydration of C-S-H gel and Ca-deficient C-S-H gel, the dehydration of $Ca(OH)_2$, and the decarbonization of $CaCO_3$30, respectively. In the case of dry weight, the mass loss over the entire temperature range is referred to as the total mass loss. The mass of $CaCO_3$ can be obtained from the CO_2 content generated by $CaCO_3$ decarbonization31. The weight-loss peak appearing in the range of 300-500 °C prior to the hydration and carbonation reaction may be caused by the formation of $Ca(OH)_2$ due to the combination of calcium-based components of LFS with atmospheric water under natural conditions. Two weight-loss peaks appeared in the range of 100 -300 °C and 500-850 °C after the hydration and carbonation reactions.

Table 2 lists the results of $CaCO_3$ and t otal mass loss measured by TG at different reaction temperatures or when different particle sizes were used, showing that the mass of $CaCO_3$ decreases with the increase in temperature or in particle size. The content of $CaCO_3$, C_2S, and C_3S was calculated by adopting the reference intensity ratio (RIR) method. Results show that, as the temperature decreases, the content of C_2S and C_3S reduces, indicating that increasing amounts of C_2S and C_3S participated in the hydration reaction stage and that, under the effect of carbonation, C-S-H gel continuously participates in the carbonation reaction stage further promoting the hydration reaction, while a reaction temperature of 20 °C is more advantageous to the occurrence of the carbonation reaction. With the increase in particle size, the content of C_2S and C_3S increase, possibly because C_2S and C_3S in LFS require longer leaching channels to participate in the hydration reaction. Furthermore, this also negatively affects the later carbonation reaction, that is, increasing particle size is not conducive to the further occurrence of the carbonation reaction.

SEM-EDS analysis of the hydration and carbonation reaction

Table 3. Elemental content of EDS areas (%)

Samples	C	O	Al	Si	Ca
20 °C	17.3	57.8	8.3	2.3	14.3
40 °C	21.7	56.7	6.0	1.1	14.6
60 °C	30.5	47.8	3.1	0.7	18.0
80 °C	15.7	55.1	5.3	1.0	23.0
96-180 μm	7.2	54.6	11.4	2.0	25.8
48-96 μm	7.7	56.0	7.6	1.0	23.3
38-48 μm	12.7	55.7	5.8	3.1	22.8
38 μm	17.3	57.8	8.3	2.3	14.3

Fig. 4 shows the SEM images of LFS following hydration and carbonation at different temperatures and when using samples of different particle sizes, Fig. 5 shows the schematic diagram of the microstructure mechanism of hydration and carbonation of a slag particle, and Table 3 lists the average elemental content of these areas according to energy-dispersive X-ray spectroscopy (EDS). As shown in Fig. 4, after hydration and carbonation, a large amount of C-S-H gel was formed with rough surfaces and a coagulated or fibrous form (indicated by the red area in Fig 4), as well as $CaCO_3$ crystals such as calcite with a cubic structure (indicated by the blue area in Fig 4) [32, 33]. As the reaction temperature increases, more voids are visible in the structure. As the particle size of the LFS increases, the amount of calcite gradually decreases, and the LFS surface is covered by C-S-H gel and Ca-deficient C-S-H gel (indicated by the green area in Fig 4). When the particle size is 96-180 μm, the hydration product $Ca(OH)_2$ is present in the form of hexagonal flakes (indicated by the yellow area in Fig 4). These results could be attributed to the cementitious properties of C_2S and C_3S, which cause a hydration reaction to form C-S-H gel and $Ca(OH)_2$. During carbonation, the C-S-H gel is decalcified to form Ca-deficient C-S-H gel and $CaCO_3$. Furthermore, $Ca(OH)_2$ directly reacts with CO_3^{2-} in solution to form $CaCO_3$. As illustrated in Figure. 5, the carbonation products $CaCO_3$ and Ca-deficient C-S-H gel adhere to the surface of the reaction phase, and the entire structure becomes dense and thus inhibits the diffusion of Ca^{2+} into the solution, which eventually prevents the further progress of the reactions. According to the results in Table 3, the reaction products are mainly composed of C, O, Al, Si, and Ca. The content of Ca gradually increases with the increase in temperature or particle size, indicating that the decalcification degree of the C-S-H gel gradually decreases, and that the concentration of Ca^{2+} ions leached into solution decreases, further reducing the formation of $CaCO_3$. As a result, increasing temperature or particle size is detrimental to the hydration and carbonation reaction.

Microstructure of the cementitious substances in the hydration and carbonation reaction

Table 4. Range of ^{29}Si NMR chemical shifts of Q_n structural units in silicate

Types	Chemical shift/ppm
Q_0	−68—−76
Q_1	−76—−82
Q_2	−82—−88
Q_3	−88—−98
Q_4	−98—−129

Table 4 shows the ^{29}Si NMR chemical shift range of Q_n structural units in silicates34, while Fig. 6 shows the ^{29}Si NMR spectra following hydration and carbonation of LFS at different temperatures or when using different LFS particle sizes. In NMR analysis, Q_0 represents an isolated SiO_4 tetrahedra, Q_1 often appears at the end group of a straight chain, Q_2 mostly appears as a middle group of a straight chain, Q_3 has a double-stranded polymer structure or a layered structure, and Q_4 represents a SiO_4 tetrahedra connected to four SiO_4 tetrahedra, in a three-dimensional network structure35. As shown in Fig. 6, the main peak of uncarbonated LFS is Q_0, with a few Q_1 peaks appearing around -79 ppm, which may be due to the formation of C-S-H gel by C_2S and C_3S hydration under natural conditions. After the hydration and carbonation reactions, Q_2, Q_3, and Q_4 peaks are present.

Table 5. Results of ^{29}Si NMR spectra deconvolution following LFS hydration and carbonation at different reaction temperatures or particle sizes

Samples	Unhydrated C-S-H gel			Ca- deficient gel		L_d	H(%)	Pol
	Q_0(%)	Q_1(%)	Q_2(%)	Q_3(%)	Q_4(%)			
Uncarbonated	93.8	6.2	-	-	-	0	6.2	0
20 °C	-	7	-	20.3	72.7	13	100	0.9
40 °C	6.7	-	18.1	51.4	23.8	4	93.3	0.8
60 °C	6.4	-	26.3	40.5	26.8	3	93.6	0.7
80 °C	46.8	-	26.9	-	26.3	1	53.2	0.5
96-180 μm	85.2	-	9.1	-	5.7	0.6	14.8	0.4
48-96 μm	-	48.6	-	46.6	4.8	1.1	100	0.5
38-48 μm	-	25.8	16.8	21.1	36.3	1.3	100	0.6
−38 μm	-	7	-	20.3	72.7	13	100	0.9

Table 5 lists the calculated deconvolution results from ^{29}Si NMR analysis. No Q_3 and Q_4 peaks are present before the hydration and carbonation reactions, indicating that it is more difficult to complete the

C_2S and C_3S hydration and carbonation reaction under natural conditions. After the hydration and carbonation reactions, the content of Q_0 gradually decreases or even disappears, and the Q_2 peak appears, indicating that at this point C_2S and C_3S begin to participate in the reaction under the action of the hydration reaction, resulting in the formation of C-S-H gel with longer chain lengths. Since the Si atom radius is smaller than the Ca atom radius, the bond length of the Si-O bond is shorter than that of the Ca-O bond, resulting in the bond energy of the Si-O bond being greater than that of the Ca-O bond. Furthermore, Si has weak non-metal properties, making it difficult to form ions alone in compounds. Therefore, as the reaction time increases, the Ca-O bonds in the C-S-H gel gradually break under the action of the carbonation reaction, and the decalcification of the C-S-H gel results in Ca^{2+} combining with CO_3^{2-} in solution to form $CaCO_3$. After decalcification, the C-S-H gel is negatively charged due to the loss of Ca^{2+}. To maintain the charge balance, H^+ in solution is adsorbed by the C-S-H gel and combines with the broken Si-O- to form -Si-OH via protonation, which subsequently undergoes a condensation reaction with the adjacent -Si-OH. This condensation increases the mean silicate chain length and forms bridges between neighboring regions, thus pulling them closer together and causing shrinkage. This results in the formation of the Q_3 and Q_4 structures of Ca-deficient C-S-H gel with longer chain lengths and a higher degree of polymerization. CS is composed of chains of SiO_4 tetrahedra (Q_2), which can directly form $CaCO_3$ during the carbonation process[11, 36]. Equations (1), (2), and (3) are used to express the degree of decalcification (L_d), the degree of polymerization (Pol) of the C-S-H gel, and the degree of hydration (H) of C_2S and C_3S, respectively[5, 37], as follows:

$$L_d = \frac{Q_3 + Q_4}{Q_1 + Q_2} \quad (1)$$

$$\mathrm{Pol} = \frac{Q_3 + Q_4}{Q_1 + Q_2 + Q_3 + Q_4} \quad (2)$$

$$\mathrm{H} = 100 - Q_0 \quad (3)$$

While H reflects the degree of C_2S and C_3S hydration, L_d reflects the degree of separation of Ca^{2+} in the C-S-H gel, Pol reflects the degree of re-polymerization of the SiO_4 tetrahedra after decalcification of the C-S-H gel. According to the results in Table 5, the ratio of Ca-deficient C-S-H gel to the remaining C-S-H gel did not change significantly in the temperature range of 40-80 °C and at particle sizes from 38 μm to 180 μm, and the decalcification degree of C-S-H gel remained low. When the reaction conditions included a temperature of 20 °C and LFS particle sizes of <38 μm, L_d was significantly increased to 13, indicating that more Ca^{2+} leached into solution, leading to more carbonation in the rapid carbonation phase. Fig. 7 shows H and Pol at different reaction temperatures and different particle sizes, indicating that, as the reaction temperature increases, both parameters exhibit a decreasing trend. This may occur as the reaction products cover the reaction phase surface, preventing further contact between water and the reaction phase, which ultimately inhibits the process of hydration. Furthermore, increasing the reaction

temperature reduces the solubility of CO_2, thereby inhibiting the carbonation reaction. The observed trend in Pol was negatively correlated with the particle size, and the reason for this analysis may be that with the decrease in particle size, the -Si-OH groups in Ca-deficient C-S-H connect more easily with adjacent Si-OH groups to form bridges and thus polymerize, thereby accelerating the carbonation reaction; released Ca^{2+} combines with CO_3^{2-} in solution to form $CaCO_3$, which will lead to a decrease in Ca^{2+} concentration; according to Kurdowski's theory, a low concentration of Ca will accelerate the hydration reaction of C_2S and C_3S and generate more C-S-H gel and Ca-deficient C-S-H gel to participate in the carbonation reaction. Therefore, the carbonation reaction promotes the hydration reaction.

Conclusions

1. According to the obtained XRD, TG-DTG, and SEM results, the hydration and carbonation reaction starts with the hydration of C_2S and C_3S to form C-S-H gel. To maintain the required alkaline environment, C-S-H gel undergoes decalcification to form Ca-deficient C-S-H gel and Ca^{2+}, and Ca^{2+} and CO_3^{2-} in solution form structurally stable $CaCO_3$. The Ca-deficient C-S-H gel undergoes a condensation reaction with adjacent -Si-OH groups to maintain charge equilibrium, resulting in a Ca-deficient C-S-H gel structure with a higher degree of polymerization of Q_3 and Q_4 units. Although increasing the temperature is beneficial to the conversion of Ca^{2+} in C_2S and C_3S, it hinders the combination of Ca^{2+} with CO_3^{2-}, thus inhibiting the hydration carbonation efficiency; increasing the particle size is not conducive to the hydration reaction of C_2S and C_3S, which in turn affects the subsequent carbonation reaction. The hydration reaction and carbonation reaction influence and promote each other.
2. The deconvolution of the ^{29}Si NMR spectra reveals that the highest degree of hydration of C_2S and C_3S, the highest effect of C-S-H gel decalcification, and the highest degree of polymerization were achieved at a temperature of 20°C, indicating that the hydration carbonation reaction was optimal at this temperature in the investigated temperature range. Moreover, the hydration of C_2S and C_3S and the polymerization of C-S-H gel decreased gradually with increasing temperature, indicating that the increase in temperature was not favorable for the hydration carbonation reaction.
3. The deconvolution of the ^{29}Si NMR spectra further indicates that the highest hydration of C_2S and C_3S and the highest decalcification and polymerization of C-S-H gel were achieved when the particle size was smaller than 38 μm, indicating that the hydration and carbonation reaction was optimal at this particle size of the investigated range. The polymerization degree of C-S-H gel decreased gradually with the increase in particle size, which increase is consequently is not conducive to the hydration and carbonation reaction.
4. For future research, the effect of cementitious substancess on the properties of LFS-based cement materials will be investigated.

Declarations

Acknowledgements

This study was funded by the National Natural Science Foundation of China (51868072).

Author Contributions

Data curation: Wenqing Ma; Methodology: Ainiwaer Sidike; Project administration: Minghang Fang; Software: Zhongle Ma; Validation: Shuqi Bai; Visualization: Yue Lin; Writing-original draft: Yuanrong Yi; Writing-review & editing: Yuanrong Yi, Yinguang Chen.

Competing Interests

The authors declare no competing financial interest or personal relationships that could have appeared to influence the work reported in this paper.

References

1. Jiang Y,Ling T C,Shi C, Pan S Y. Characteristics of steel slags and their use in cement and concrete—A review.[J] Resources, Conservation and Recycling, 2018. 136: p. 187–197.http://dx.doi.org/https://doi.org/10.1016/j.resconrec.2018.04.023
2. Yi Y-R. *et al*. Accelerated carbonation of ladle furnace slag and characterization of its mineral phase. [J] Construction and Building Materials, 2021. 276.http://dx.doi.org/10.1016/j.conbuildmat.2020.122235
3. Adolfsson D,Menad N,Viggh E, Björkman B. Steelmaking slags as raw material for sulphoaluminate belite cement.[J] Advances in Cement Research, 2007. 19(4): p. 147–156.http://dx.doi.org/10.1680/adcr.2007.19.4.147
4. Araos Henríquez P,Aponte D, Ibáñez-Insa J, Barra Bizinotto M. Ladle furnace slag as a partial replacement of Portland cement.[J] Construction and Building Materials, 2021. 289.http://dx.doi.org/10.1016/j.conbuildmat.2021.123106
5. Gaitero J J, Campillo I, Guerrero A. Reduction of the calcium leaching rate of cement paste by addition of silica nanoparticles.[J] Cement and Concrete Research, 2008. 38(8): p. 1112–1118.http://dx.doi.org/10.1016/j.cemconres.2008.03.021
6. Pan S Y,Liu H L,Chang E E,Kim H, Chiang P C. Multiple model approach to evaluation of accelerated carbonation for steelmaking slag in a slurry reactor.[J] Chemosphere, 2016. 154: p. 63–71.http://dx.doi.org/https://doi.org/10.1016/j.chemosphere.2016.03.093
7. 7.. Xu B, Yi Y. Treatment of ladle furnace slag by carbonation: Carbon dioxide sequestration, heavy metal immobilization, and strength enhancement.[J] Chemosphere, 2021. 287(Pt 3): p. 132274.http://dx.doi.org/10.1016/j.chemosphere.2021.132274
8. Monkman S,Shao Y, Shi C. Carbonated Ladle Slag Fines for Carbon Uptake and Sand Substitute.[J] Journal of Materials in Civil Engineering, 2009. 21(11): p. 657–665.http://dx.doi.org/https://doi.org/10.1061/(ASCE)0899-1561(2009)21:11(657)

9. Auroy M. *et al*. Comparison between natural and accelerated carbonation (3% CO_2): Impact on mineralogy, microstructure, water retention and cracking.[J] Cement & Concrete Research, 2018. 109: p. 64–80.http://dx.doi.org/10.1016/j.cemconres.2018.04.012
10. Wouter. *et al*. Mineral CO_2 Sequestration by Steel Slag Carbonation.[J] Environmental Science & Technology, 2005. 39(24): p. 9676–9682.http://dx.doi.org/10.1021/es050795f
11. Ashraf W, Olek J. Carbonation behavior of hydraulic and non-hydraulic calcium silicates: potential of utilizing low-lime calcium silicates in cement-based materials.[J] Journal of Materials Science, 2016.http://dx.doi.org/10.1007/s10853-016-9909-4
12. Reddy K R. *et al*. Effect of basic oxygen furnace slag particle size on sequestration of carbon dioxide from landfill gas.[J] Waste Management & Research, 2019. 37(5): p. 0734242X1882394.http://dx.doi.org/10.1177/0734242X18823948
13. Zhang T,Yu Q,Wei J,Li J,Zhang P. Preparation of high performance blended cements and reclamation of iron concentrate from basic oxygen furnace steel slag.[J] Resources Conservation & Recycling, 2011. 56(1): p. 48–55.http://dx.doi.org/10.1016/j.resconrec.2011.09.003
14. Suh H, A. *et al*. Influences of rehydration conditions on the mechanical and atomic structural recovery characteristics of Portland cement paste exposed to elevated temperatures.[J] Construction and Building Materials, 2019. 235.http://dx.doi.org/10.1016/j.conbuildmat.2019.117453
15. Liu W,Li Y Q,Tang L P,Dong Z J. XRD and ^{29}Si MAS NMR study on carbonated cement paste under accelerated carbonation using different concentration of CO_2.[J] Materials Today Communications, 2019. 19.http://dx.doi.org/10.1016/j.mtcomm.2019.05.007
16. S. Song D S, H. M, Jennings & T. O. Mason. Hydration of alkali-activated ground granulated blast furnace slag.[J] Journal of Materials Science 2000. 35,: p. 249–257.http://dx.doi.org/https://doi.org/10.1023/A:1004742027117
17. Khan M,Kayali O.Troitzsch U. Effect of NaOH activation on sulphate resistance of GGBFS and binary blend pastes.[J] Cement and Concrete Composites, 2017: p. 49–58.http://dx.doi.org/10.1016/j.cemconcomp.2017.04.007
18. Maddalena R,Li K,Chater P A,Michalik S, Hamilton A. Direct synthesis of a solid calcium-silicate-hydrate (C-S-H).[J] Construction and Building Materials, 2019. 223(2019): p. 554–565.http://dx.doi.org/10.1016/j.conbuildmat.2019.06.024
19. Yang K H, Song J K. Workability Loss and Compressive Strength Development of Cementless Mortars Activated by Combination of Sodium Silicate and Sodium Hydroxide.[J] Journal of Materials in Civil Engineering, 2009. 21(3): p. 119–127.http://dx.doi.org/doi.org/10.1061/(ASCE)0899-1561(2009)21:3(119)
20. Li Q,Hurt A P, Coleman N J. The Application of 29Si NMR Spectroscopy to the Analysis of Calcium Silicate-Based Cement using Biodentine as an Example.[J] Journal of Functional Biomaterials, 2019. 10(2).http://dx.doi.org/10.3390/jfb10020025
21. Ma H, Li Z. Multi-scale modeling of the microstructure of concrete. in The Twenty-Fourth KKCNN Symposium on Civil Engineering. 2011.

22. Chen J J,Thomas J J, Jennings H M. Decalcification shrinkage of cement paste.[J] Cement and Concrete Research, 2006. 36(5): p. 801–809.http://dx.doi.org/10.1016/j.cemconres.2005.11.003
23. Fang Y, Chang J. Microstructure changes of waste hydrated cement paste induced by accelerated carbonation.[J] Construction & Building Materials, 2015. 76(feb.1): p. 360–365.http://dx.doi.org/10.1016/j.conbuildmat.2014.12.017
24. Reddy K R,Gopakumar A,Chetri J K,Kumar G, Grubb D G. Sequestration of Landfill Gas Emissions Using Basic Oxygen Furnace Slag: Effects of Moisture Content and Humid Gas Flow Conditions.[J] Journal of Environmental Engineering, 2019. 145(7).http://dx.doi.org/10.1061/(ASCE)EE.1943-7870.0001539
25. Ashraf W,Olek J, Atakan V. A Comparative Study of the Reactivity of Calcium Silicates during Hydration and Carbonation Reactions. in 14th International Congress on the Chemistry of Cement (ICCC 2015). 2015.
26. Jang J G, Lee H K. Microstructural densification and CO_2 uptake promoted by the carbonation curing of belite-rich Portland cement.[J] Cement & Concrete Research, 2016. 82: p. 50–57.http://dx.doi.org/10.1016/j.cemconres.2016.01.001
27. Ashraf W,Olek J, Sahu S. Phase evolution and strength development during carbonation of low-lime calcium silicate cement (CSC).[J] Construction and Building Materials, 2019. 210: p. 473–482.http://dx.doi.org/10.1016/j.conbuildmat.2019.03.038
28. Pan S-Y,Chang E E, Chiang P-C. CO_2 Capture by Accelerated Carbonation of Alkaline Wastes: A Review on Its Principles and Applications.[J] Aerosol and Air Quality Research, 2012. 12(5): p. 770–791.http://dx.doi.org/10.4209/aaqr.2012.06.0149
29. Chang E E,Chen C-H,Chen Y-H,Pan S-Y, Chiang P-C. Performance evaluation for carbonation of steel-making slags in a slurry reactor.[J] Journal of Hazardous Materials, 2011. 186(1): p. 558–564.http://dx.doi.org/https://doi.org/10.1016/j.jhazmat.2010.11.038
30. Wang D, Chang J. Comparison on accelerated carbonation of β-C_2S, $Ca(OH)_2$, and C_4AF: Reaction degree, multi-properties, and products.[J] Construction and Building Materials, 2019. 224: p. 336–347.http://dx.doi.org/10.1016/j.conbuildmat.2019.07.056
31. Santos A. *et al*. Larnite powders and larnite/silica aerogel composites as effective agents for CO_2 sequestration by carbonation.[J] Journal of Hazardous Materials, 2009. 168(2–3): p. 1397–1403.http://dx.doi.org/10.1016/j.jhazmat.2009.03.026
32. Chang J,Fang Y,Shang X,Wang J. Effect of accelerated carbonation on microstructure of calcium silicate hydrate.[J] Journal of the Chinese Ceramic Society, 2015. 43(8): p. 1055–1060.http://dx.doi.org/10.14062/j.issn.0454-5648.2015.08.06
33. De Beer M,Doucet F J,Maree J P, Liebenberg L. Synthesis of high-purity precipitated calcium carbonate during the process of recovery of elemental sulphur from gypsum waste.[J] Waste Management, 2015. 46(DEC.): p. 619–627.http://dx.doi.org/10.1016/j.wasman.2015.08.023

34. Lippmaa E,Maegi M,Samoson A,Engelhardt G, Grimmer A R. Structural studies of silicates by solid-state high-resolution ^{29}Si NMR.[J] Journal of the American Chemical Society, 1980. 102(15): p. 4889–4893.http://dx.doi.org/10.1021/ja00535a008
35. Feng C,Wang X, Li D. Application progress of solid ^{29}Si, ^{27}Al NMR in the research of cement-based materials.[J] He Jishu/Nuclear Techniques, 2014. 37(1): p. 010502–010505.http://dx.doi.org/10.11889/j.0253-3219.2014.hjs.37.010502
36. Hansen M R,Jakobsen H J, Skibsted J. ^{29}Si Chemical Shift Anisotropies in Calcium Silicates from High-Field ^{29}Si MAS NMR Spectroscopy.[J] Inorganic Chemistry, 2003. 42(7): p. 2368–2377.http://dx.doi.org/10.1021/ic020647f
37. Bosque I F S e d,Martı´n-Pastor M,Martı´nez-Ramı´rez S, TeresaBlanco-Varela M a. Effect of Temperature on C_3S and C_3S + Nanosilica Hydration and C–S–H Structure.[J] Journal of the American Ceramic Society, 2013. 96(3).http://dx.doi.org/10.1111/jace.12093

Figures

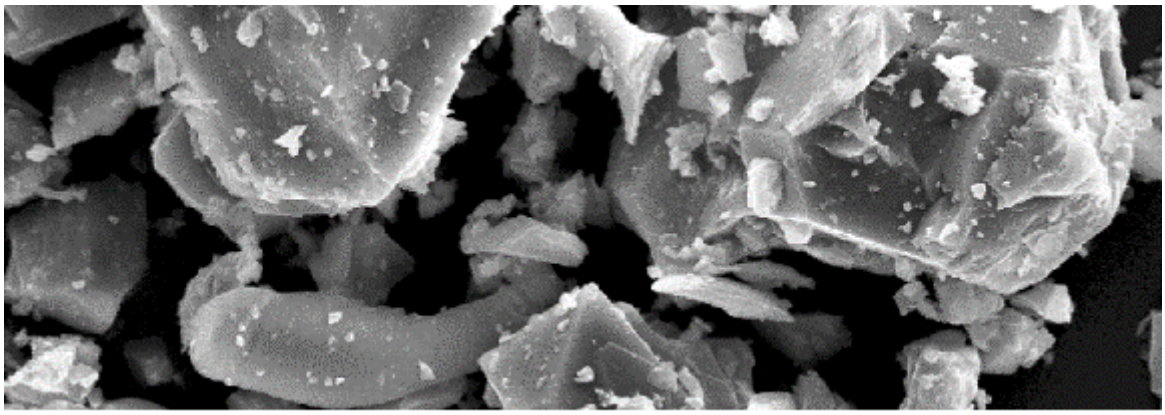

Figure 1

Micrograph of the original LFS

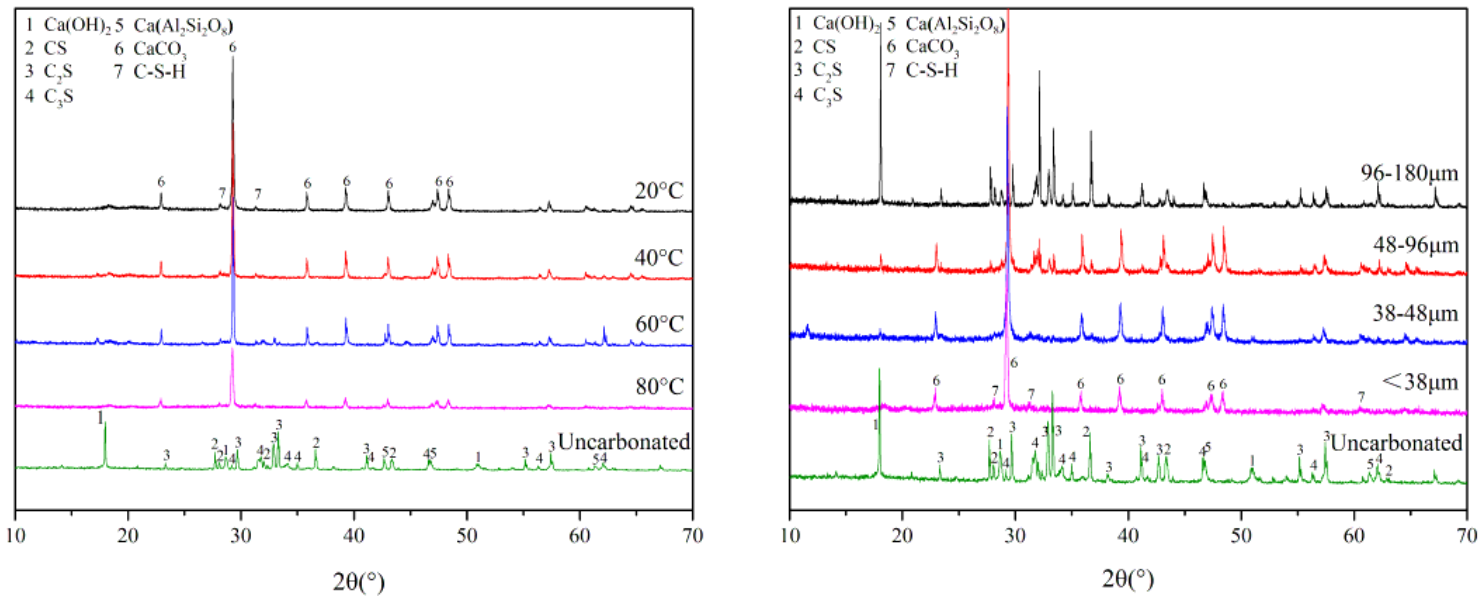

Figure 2

XRD patterns of original LFS and LFS samples after hydration and carbonation at different reaction temperatures or particle sizes

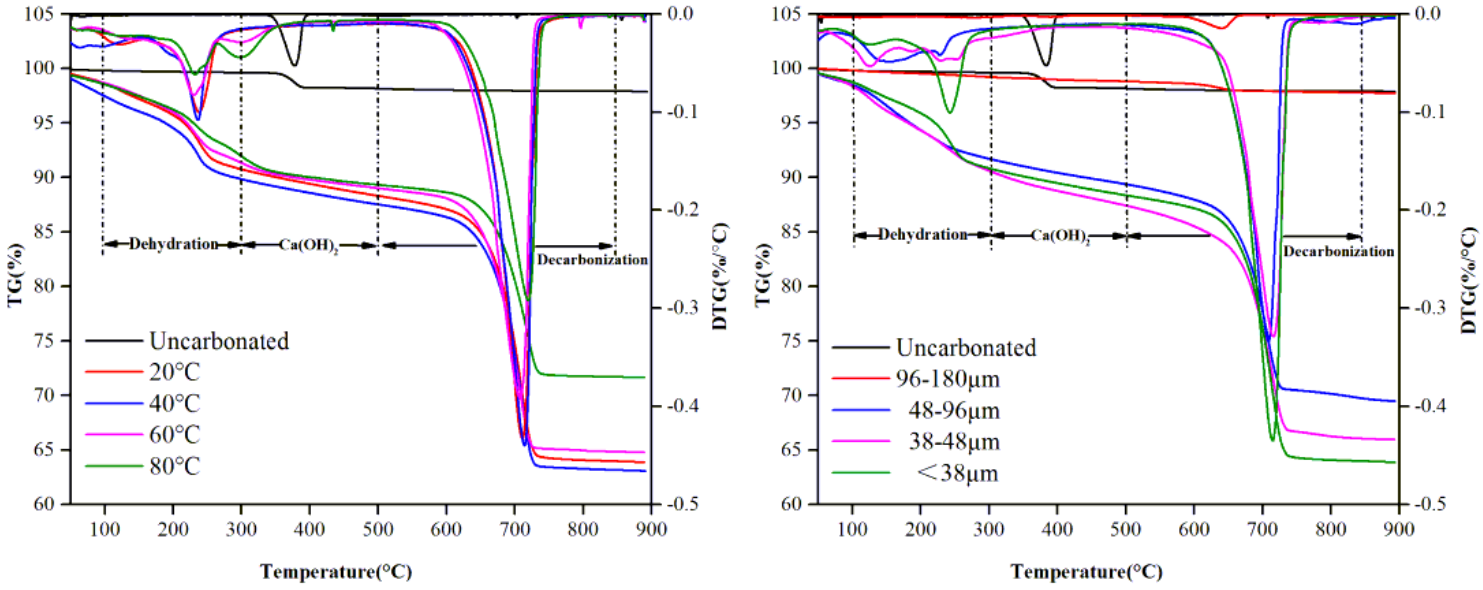

Figure 3

TG-DTG diagrams of original LFS and LFS samples after hydration and carbonation at different temperatures or particle sizes

Figure 4

SEM images of LFS materials following hydration and carbonation at different temperatures or different LFS particle sizes

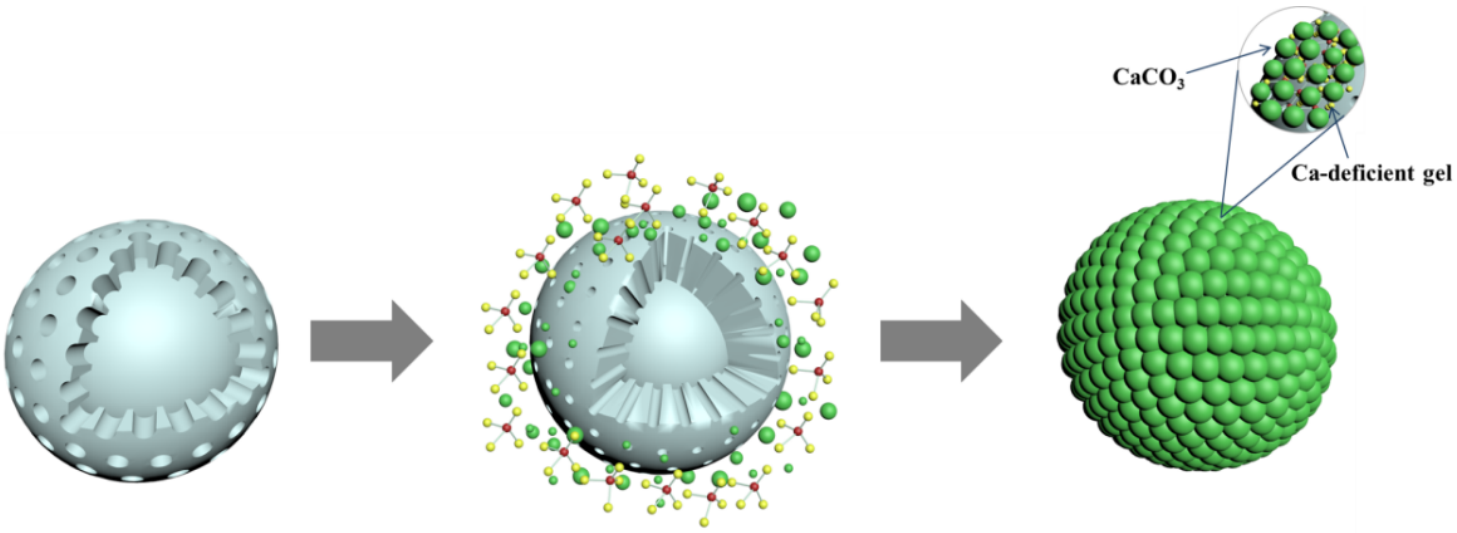

Figure 5

Schematic diagram of the microstructure mechanism of hydration and carbonation of LFS

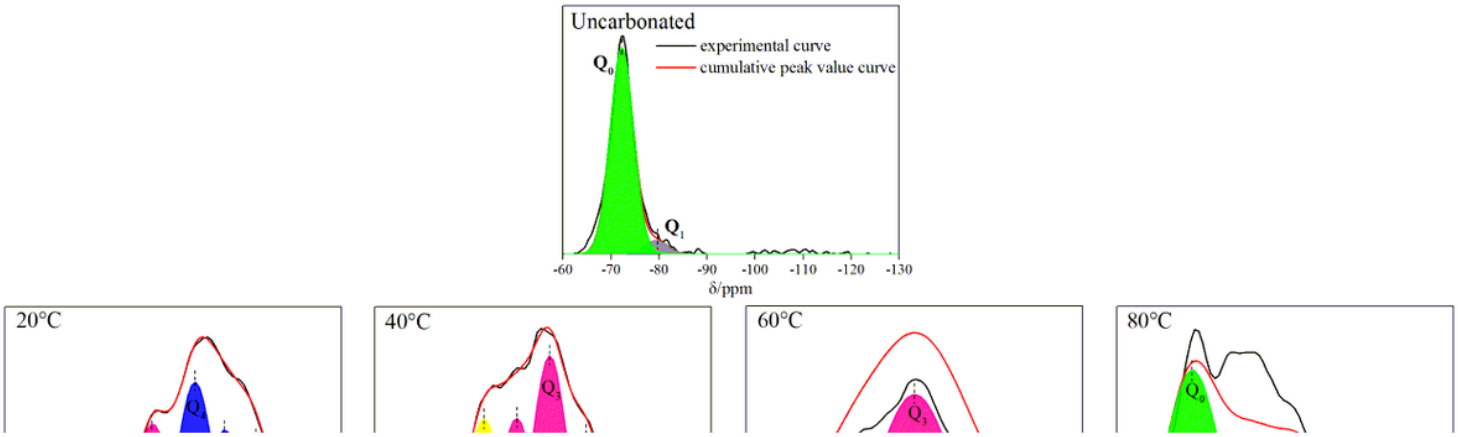

Figure 6

^{29}Si NMR spectr a of original LFS and LFS samples after hydration and carbonation at different temperatures or different particle sizes

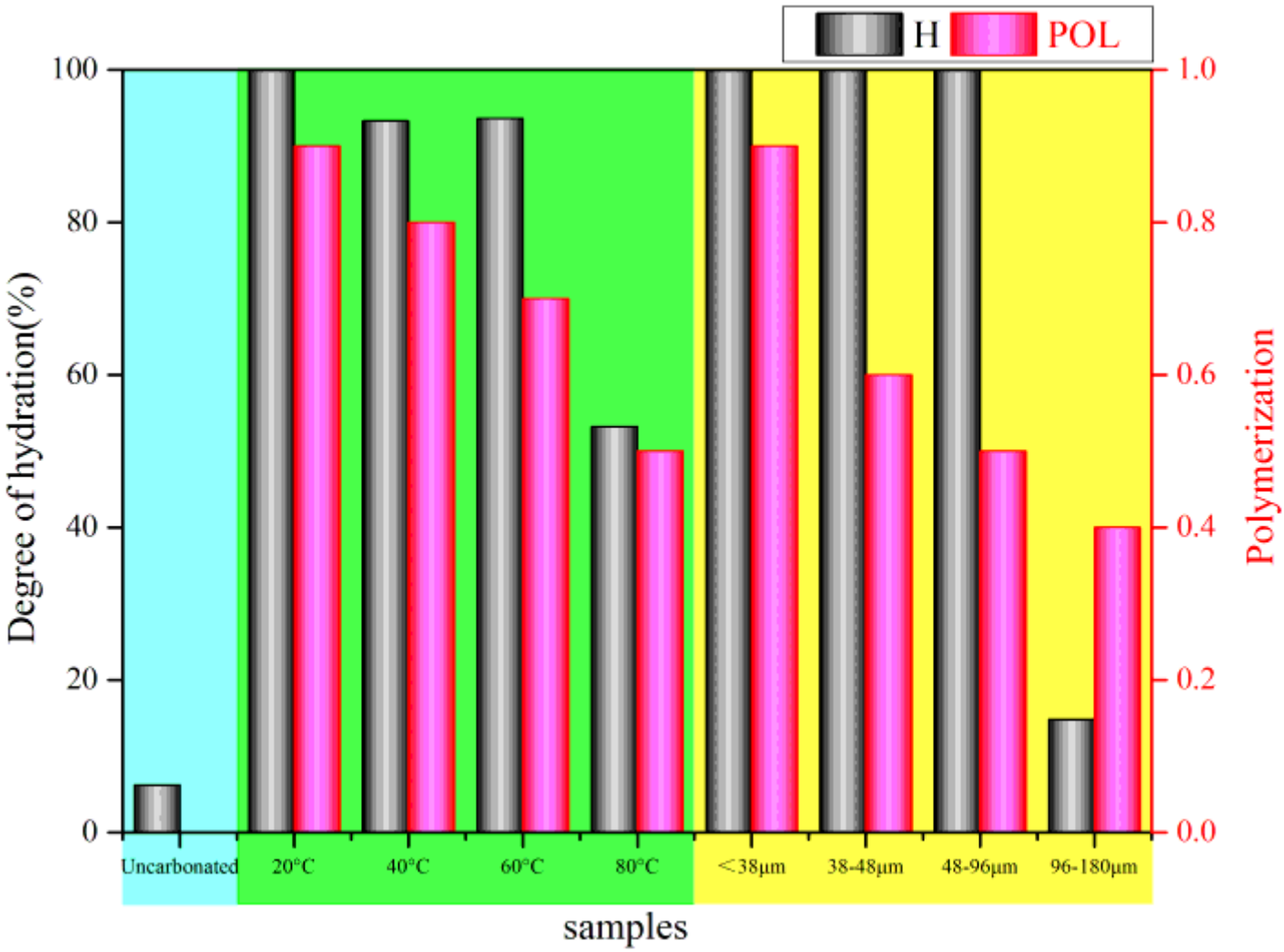

Figure 7

Hydration and polymerization degree of C_2S and C_3S at different reaction temperatures or different particle sizes

Supplementary Files

This is a list of supplementary files associated with this preprint. Click to download.

- Onlinefloatimage1.png